Hindawi
International Journal of Rotating Machinery
Volume 2022, Article ID 9772362, 15 pages
https://doi.org/10.1155/2022/9772362

Research Article

Modelling of Hydroabrasive Erosion in Pelton Turbine Injector

Tri Ratna Bajracharya,[1,2] **Rajendra Shrestha**,[1] **Anil Sapkota**,[1,2] **and Ashesh Babu Timilsina**[1,2]

[1]*Department of Mechanical and Aerospace Engineering, Pulchowk Campus, Institute of Engineering, Tribhuvan University, Nepal*
[2]*Center for Energy Studies, Institute of Engineering, Tribhuvan University, Nepal*

Correspondence should be addressed to Ashesh Babu Timilsina; abtimilsina@pcampus.edu.np

Received 30 December 2021; Accepted 4 July 2022; Published 31 July 2022

Academic Editor: Abraham Engeda

Sand particle-led erosion in the turbine parts of hydropower projects (excluding storage type projects) based on Himalaya-originated Rivers is one of the key operational challenges for concerned hydropower stations. Researchers have made multiple attempts to understand the nature of erosion and its combating technique by using numerical and experimental modelling techniques. This study relates to numerical and experimental modelling of sand particle-led erosion in the injector of the most preferred high head turbine, i.e., the Pelton turbine, followed by a comparative analysis of both techniques. This article attempts to compare erosion qualitatively and quantitatively, thus adding to the current state of the art of turbine erosion modelling. The results direct that the erosion-prone area is the needle seat in the nozzle and the region between the needle tip and nozzle exit in the needle, similar to findings reported by authors performing field setting research. The innovative aspect of the study is that by mapping the shape of the initial and eroded needle, mass lost in the erosion-prone area (as indicated by numerical erosion modelling) is calculated and compared against numerical modelling results. With the Oka erosion model employed for numerical modelling, the error in computation is about 31%. The nature of erosion in a partially open injector reveals that erosion in the needle increases with the nozzle's partial opening. Nozzle erosion spreads away from the needle seat to the whole nozzle body. As commonly understood, the erosion of turbine parts gives rise to mechanical vibrations (especially in rotating parts) and energy loss. Numerical modelling results of injector erosion's effect on jet energy are also presented. With uniformly spread erosion of 0.5 mm in both the needle and nozzle, loss in jet energy is 5.63%.

1. Introduction

Globally, river systems originating from the Himalayas and the Andes are sediment loaded with the domination of hard minerals such as quartz and feldspar [1, 2]. Such sediment loading is high during the summer season and low during the winter season [2–4]. The detailed quantitative study of sediment content gives an insight into the seasonal variation of the sediment content in these rivers. A specific case study by Chhetri et al. [5] on one of the rivers originating in the Himalayas, the Langtang River, reveals seasonal variation with sediment loading data as follows:

(i) Pre-monsoon: 37.69 tons per day

(ii) Post-monsoon: 11.52 tons per day

(iii) Highest value: 872.86 tons per day (monsoon season)

(iv) Lowest value: 5.54 tons per day (winter season)

Despite installing well-engineered arrangements, like gravel traps and desanding basins, to trap the sediments, fine-sized sediments (diameter < 2 mm) make their way into the hydromechanical parts. This entrainment causes severe hydroabrasive erosion in hydromechanical parts [6–8]. Sediment-induced wear in the hydraulic machinery is one of the critical problems in the hydropower plant's operation and maintenance (O&M). Hydroabrasive erosion is an economically important issue because of a decrease in revenue due to loss of efficiency and increased cost associated with the maintenance of eroded parts [9].

In a Pelton turbine, the core components are the injector assembly and the runner assembly. The injector interacts with the water, often sediment-laden, incoming from the penstock and converts the potential energy of the water to kinetic energy. The impact of sand particles on the water-solid interface is known as solid particle impingement. This impingement of hard solid particles on the turbine parts causes erosive wear on the injector assembly and buckets. It introduces undesired altercations in the needle/nozzle and buckets surface profile. These altercations reduce the turbine performance and raise the risk of breakage or damage.

On the other hand, these phenomena might affect jet velocity distribution and shape and lead to undesired secondary flows, lowering the nozzle velocity coefficient, injector efficiency, and system efficiency. Hence, erosion is a matter of grave concern in the Pelton turbine. Predicting the eroded shape and the inception of sand particle-led erosion is imperative to ensure the safe operation of the hydroelectric project. It is equally important to understand the erosion mechanisms for making design, surface morphology, and material changes to reduce the effect of sediment particles.

The Pelton turbine is broadly divided into four parts to study erosion and design a unit for working in sediment-laden water: the inlet system, the nozzle system, the runner, and the turbine pits [10]. Bajracharya et al. [11] have provided a detailed and extensive literature review on hydroabrasive erosion and flow modelling in Pelton turbine injectors.

Before numerically predicting the erosion pattern and establishing its effects on the system efficiency and longevity, it is essential to study the flow in the injector assembly and its variation with injector geometry (needle-nozzle angles and opening). Owing to the inherent complex flow regime in the injector and gradual development of CFD codes, the first successful approach to numerically model the Pelton turbine jet flow took place in 1996. Assuming an axisymmetric jet, Nonoshita et al. [12] concluded that needle stroke and head change the velocity distribution in the jet. An experimental study by Staubli and Hauser [13] accommodated the variation of jet flow with needle stroke (nozzle opening). The same study concluded that the jet diameter decreases along with the decrease in nozzle opening, as studied by photographic observations.

Similarly, Peron et al. [14] numerically modelled the flow through the Pelton turbine injector considering upstream bends for investigating the phenomenon of jet dispersion. The authors have modified the flow path upstream of the injector to make the flow more streamlined, thus reducing the formation of vortices and jet dispersion and increasing overall unit efficiency. Likewise, Gupta and Prasad [15] numerically modelled flow through the injector, considering injector geometry only. Keeping spear geometry the same, the authors studied different nozzle geometry (needle-nozzle geometry) and recommended optimal geometry. There is an alteration in jet quality; hence, the energy content was delivered to the Pelton buckets due to erosion in the needle-nozzle surface. An experimental study using Laser Doppler Anemometry (LDA) method [16] reveals the jet's velocity distribution, which matches the one from the computational studies mentioned above.

Bajracharya [17] did the first dedicated study on Pelton turbine hydroabrasive erosion. The experimental study concluded that with sand particle-led erosion, the efficiency of a Pelton turbine unit deteriorates, and the rate of deterioration is directly related to the operating hours and sand particle concentration. A field setting research with an 11 MW unit revealed an efficiency loss of 1.21% within a year [3]. Neopane et al. [18] reviewed erosion in hydraulic turbines and identified and discussed the erosion in different hydraulic turbine areas.

The needle seat, needle, and bucket are the most vulnerable to hydroabrasive erosion [18]. The splitter and bucket surface are the parts most susceptible to hydroabrasive erosion for a Pelton bucket. Similarly, ANDRITZ Hydro [19] conducted field-setting research to study HVOF coatings to tackle hydroabrasive erosion and concluded that the needle is four times more long-lasting with the coating (steel coated with SXHTM 48). Morales et al. [20] experimentally studied the effect of coatings (HVOF and plasma nitriding process) on needle erosion in field research. The research concluded that coated needles have a longer life.

Stepping on the works of Bajracharya [17], Chongji et al. [21] and Chongji et al. [22] made the first attempt at sand particle-led erosion modelling of Pelton turbine injector using a commercial CFD code based on the FVM technique. The authors later discovered that large particles have more potential for erosion [21]. Messa et al. [23] further studied the hydroabrasive erosion in Pelton turbine injectors using a commercial CFD code STAR CCM+. The study compares DNV and Oka erosion models that neglect cavitation in the flow domain, which shows that the Oka model better predicted the erosion pattern. Since these three pieces of literature do not incorporate experiments, any claims on error approximations of erosion prediction are not adequately represented. Recently, Jung et al. [24] studied the loss of efficiency due to needle-nozzle eccentricity. The study shows that eccentricity is critical in power loss for small Pelton turbines in partially opened conditions.

Multiple pieces of literature have reviewed Pelton turbine erosion with different conclusive results [3, 4, 17, 18, 20–22, 25]. Figure 1 shows typical erosion areas in a Pelton turbine.

Židonis and Aggidis [26] reviewed the numerical modelling of the Pelton turbine. They concluded that ANSYS Fluent is the preferred code for jet flow among researchers, while CFX is the choice for jet-bucket interaction study. Similarly, Smoothed Particle Hydrodynamics (SPH) is another numerical approach for modelling fluid flow along with the Finite Volume Method (FVM). However, SPH solver accuracy is a significant concern, as seen in the literature that has adapted this code for numerical study. Papantonis et al. [27] studied the scope of SPH to model flow in Pelton turbine injectors. The authors successfully implemented the SPH technique to model the flow through the Pelton turbine injector without conclusive results.

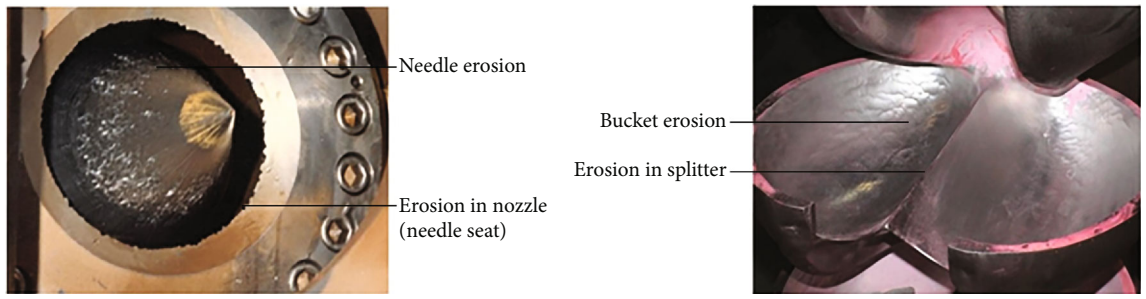

Figure 1: Typical erosion in Pelton turbine parts: (a) Mel Norway [18] and (b) bucket of Khimti Powerplant, Nepal [4].

Recent advances in computational techniques and computing hardware have enabled CFD-based modelling to examine jet flow in Pelton turbines and forecast erosion. However, it is unclear which erosion models will accurately forecast erosion in the Pelton turbine injector and flow change after erosion. Field observations, experiments, numerical simulations, and comparison of the results can help better understand the mechanics involved in solid particle impingement in the Pelton turbine injector and the most appropriate erosion model to anticipate this mechanism.

To summarise, the early flow studies in the Pelton turbine were based on trials and experiments of which fewest publications are available. Later, systematic laboratory-based investigations of jet flow and injector erosion started. After gradual development in CFD, computational flow and erosion modelling in the Pelton turbine injector started. However, the studies are limited to experimental (or field-based) or computational. None of the research was a combination of experimental and computational studies. Bajracharya [17] studied the erosion in the Pelton turbine injector with the actual erosion data of the Chilime Hydropower Plant of Nepal. It can be inferred that CFD-based erosion modelling of the hydroturbine was a nascent technique back then.

The first approach for CFD-based approach for erosion modelling was by Chongji et al. [22], followed by Chongji et al. [21]. However, these purely computational studies used the results of Bajracharya [17] to compare their computational approach to erosion modelling. Likewise, Messa et al. [23] made further improvements and performed CFD-based erosion modelling of the Pelton turbine injector without any experimental modelling.

In this study, neglecting the occurrence of cavitation in the flow domain, numerical, and experimental hydroabrasive erosion modelling in the Pelton turbine injector has been undertaken and compared. The central innovative aspect is that the brass is taken as turbine material and studied for erosion for the same geometry and sand particle properties. The primary goal is to improve the present ability to model flow and sand particle-induced erosion in the Pelton turbine injector (also applicable for needle valves).

As the literature suggests, a half-open injector is more prone to erosion, and the Oka model is the more fitting to predict erosion [3, 23]. Thus, obtained erosion rate density is compared against the experimental results. The experimental and the computational results are compared against field research for erosion patterns and erosion-prone areas. After that, the adverse effect of erosion on jet flow (energy content of jet) is examined and discussed. Most research has compared their results to other's experiments to verify their modelling approaches among the published literature on numerical modelling of the Pelton turbine injector. Studies based on this approach are lacking in quantitative comparison. It can be argued that a proper correlation between the numerical model and laboratory-based experiments has not been established.

This study takes this lack of proper correlation as a stepping stone, and a methodology is proposed to address this issue. Also, a handful of publications on the numerical and the experimental modelling of the Pelton turbine injector necessitate this research. Furthermore, this is also applicable to needle valves (needle valves are commonly used as a bypass valve for spiral case filling in the Francis turbine system).

2. Methodology

The numerical modelling approach adopted in this study is similar to Chongji et al. [21], Messa et al. [23], and Chongji et al. [22]. However, the authors have not mentioned the sand sample taken for the research but compared their findings with field setting research, which has operated on different sand samples and needle geometry. Thus, the methodology is designed to use the same sand sample for controlled testing in the test rig and the CFD-based erosion modelling. Figure 2 shows the flow of the study, different tasks undertaken, and their interconnection.

The test rig, previously used by Bajracharya [17], underwent a complete overhaul to ensure no leakage and fully functioning components. Then, a CAD model and a mesh were developed for the injector geometry to be studied computationally. After collecting the sand sample from desanding basin outlet of Chilime HPP, experiments were performed on the test rig and computational erosion modelling was conducted based on the particle size distribution (PSD) data.

2.1. Experimental Modelling

2.1.1. Test Rig. The test rig used in this study was designed and developed by Bajracharya [17]. Figure 3 shows the test rig,

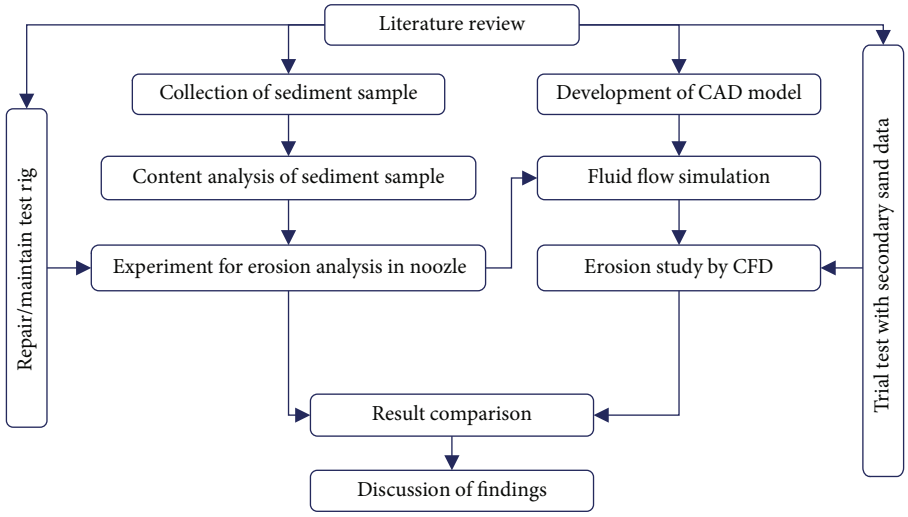

Figure 2: Methodology.

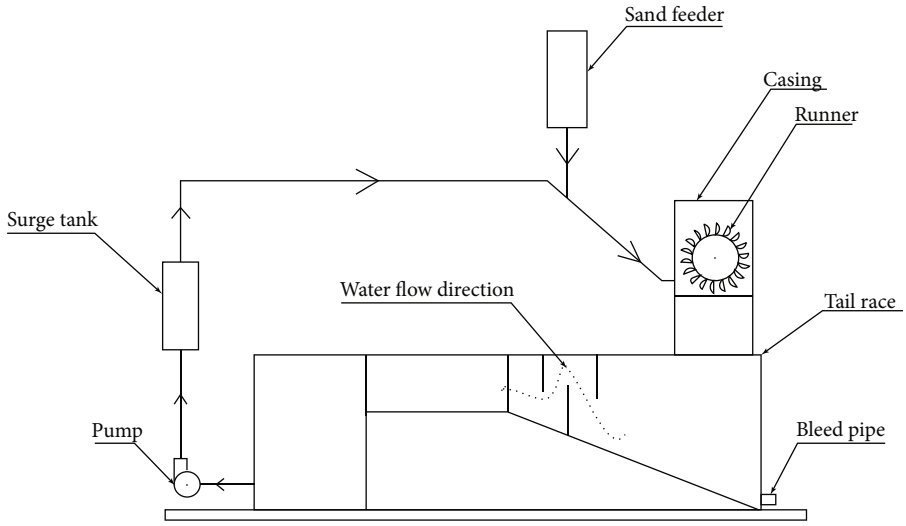

(a)

(b)

Figure 3: (a) Schematic of the test rig and (b) the test rig used in the study previously used by Bajracharya [17].

which is a dry sand type test rig. The pump creates the required head and flow, whereas the sand feeder mixes the sand at a controlled rate to the penstock pipe using an extruder mechanism. The slurry then passes through the injector to strike the turbine. After hitting the bucket, the slurry water descends to the tailrace, which separates the sand particle from water as the water

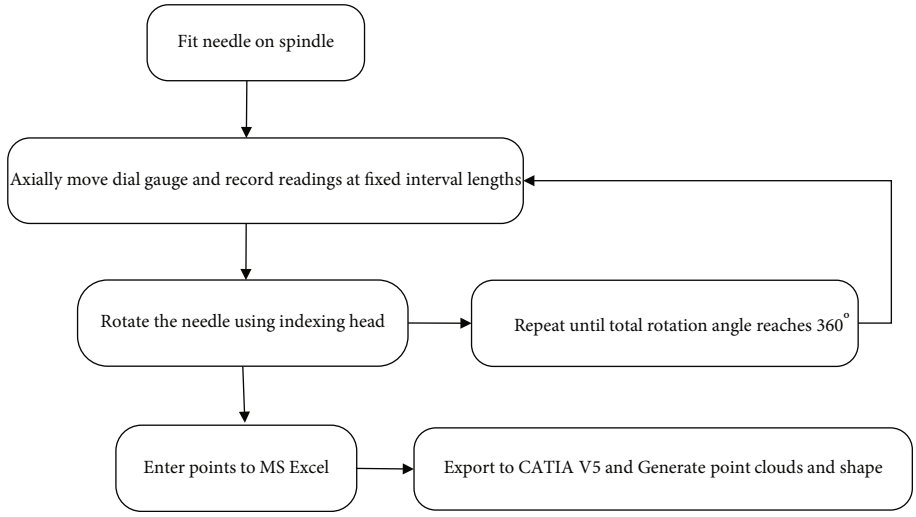

Figure 4: Methodology to record needle profile.

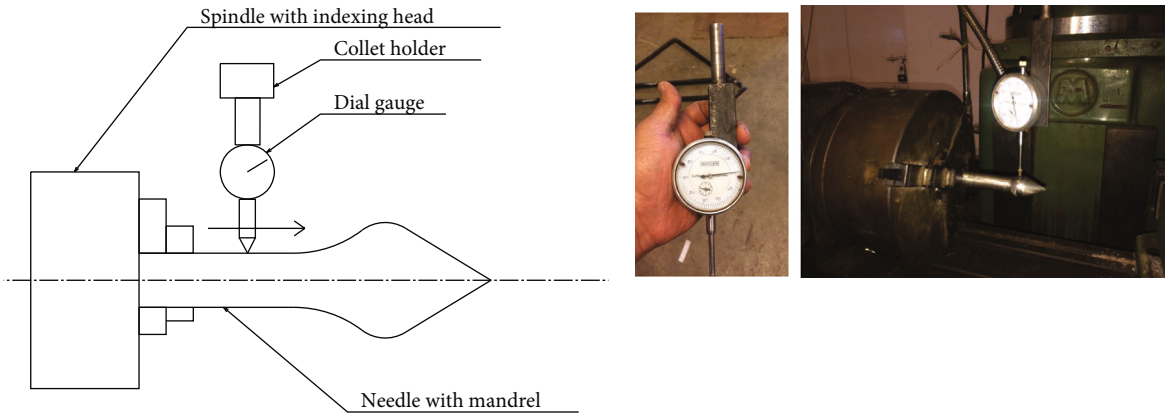

Figure 5: Measurement setup schematic on (a) and snapshot of profile measurement with dial gauge fixture on (b).

passes through the baffle plates towards the suction chamber of the pump. The 6.3 kW pump is centrifugal, manufactured by Kirloskar (Model No: KDS-852++), with a discharge and head capacity of 0.006 m^3/s and 46 m, respectively. It fits the commercially available GI pipe of 2 ∗ 1/2 inches, and the internal diameter of the penstock pipe is 68 mm. A worm gear rotates the feeding screw mounted at hopper/sand tank assembly and a bypass jet from the penstock pipe. The speed of the screw is adjusted to control the sediment concentration of inflowing water. A camera mounted inside the casing captures the jet flow and jet-bucket interaction.

2.1.2. Needle Profile Measurement. Few attempts have been made for the experimental measurement of erosion. The idea is to track weight loss [17] with results obtained in mass loss per unit time or by measuring eroded profile [3] with results obtained in thickness loss per unit time. This method proposed is a slight development from both previous approaches. The eroded shape is measured in three dimensions (3D), and mass lost is calculated based on the eroded profile. The idea is to measure the initial profile of the object and create a 3D geometry based on the measured values. Then, the entity is subjected to sand-particle laden water for erosion.

Precautions were taken to ensure no alteration in the position during measurement and installation in the test rig by using positional marks (matching marks between detachable components) and mandrels (for measurement). Authors realise that alteration of position produces a substantial measurement error. Thus, the same angular position was ensured during installation in the test rig and measurement of the surface profile of the injector needle.

Figure 4 shows the iterative measurement process for initial and eroded profiles. As shown in Figure 5, a dial gauge moves axially along the needle surface. The dial gauge fixture was devised and set on a milling machine. The complete needle profile is obtained by rotating a fixed degree each time with the index head after a profile is obtained at a particular angular position. The Figure 6(a) is the needle profile at 0°. After

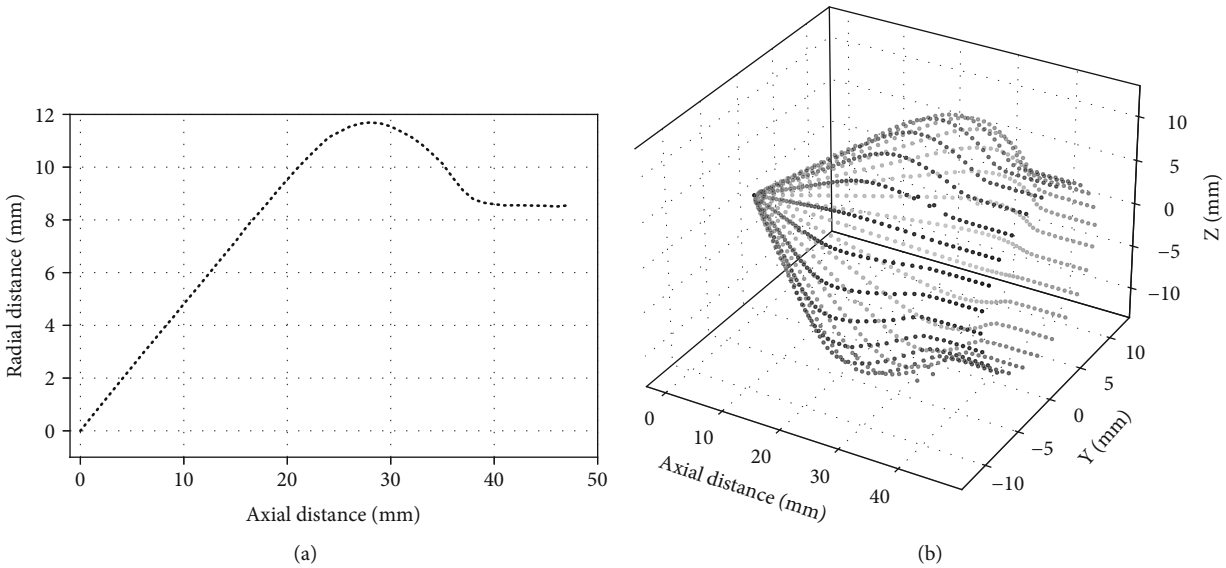

Figure 6: Initial readings of needle shape.

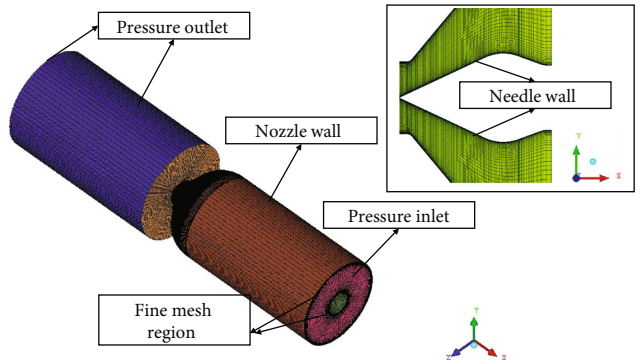

Figure 7: Mesh with inflation layers on walls and respective boundary conditions.

Table 1: Solver settings used in ANSYS Fluent.

Solver	3D, steady state, pressure based	Convergence criteria	RMS, scaled residual target = $10E-6$
Hardware	Processor: Intel Core i7 @ 3.6 GHz (8 CPUs), memory: 32 GB	Discretisation scheme	Second-order upwind
		Turbulence model	Realisable k-epsilon

rotating 15°, again, a set of readings was taken. Twenty-four sets of such profile readings were generated and used to create the complete needle profile (Figure 6(b)). A macro exported the readings from MS Excel to CATIA as point cloud data to create an entire surface. After certain hours of operation, the needle in sediment-laden water undergoes erosion which changes the initial profile. The cloud point data was recorded for the eroded needle by repeating the same measurement procedure with a dial gauge, and the shape was developed in CATIA. The comparative study of the shapes helps identify the erosion-prone area and the eroded shape.

2.2. Computational Modelling. The process in a study with CFD simulation is readying the flow domain with geometry

Table 2: Mesh discretisation error summary based on Celik et al. [28].

Parameter	ϕ = jet velocity ($m.s^{-1}$)	ϕ = erosion rate density ($\times 10^{-3}$ $kg.m^{-2}.s^{-1}$)
$N_1; N_2; N_3$	1,423,800; 709,400; 352,200	
$r = r_{21} = r_{32}$	1.26	
ϕ_1, ϕ_2, ϕ_3	24.52, 24.50, 24.42	3.09, 3.05, 2.90
p	5.9984	5.7191
$\phi^{21}_{ext}, \phi^{32}_{ext}$	24.5267, 24.5267	3.1045, 3.1045
e^{21}_{a}, e^{32}_{a}	0.08%, 0.33%	1.29%, 4.92%
$e^{21}_{ext}, e^{32}_{ext}$	0.03%, 0.11%	0.47%, 1.76%
$GCI^{21}_{fine}, GCI^{32}_{fine}$	0.03%, 0.14%	0.59%, 2.24%

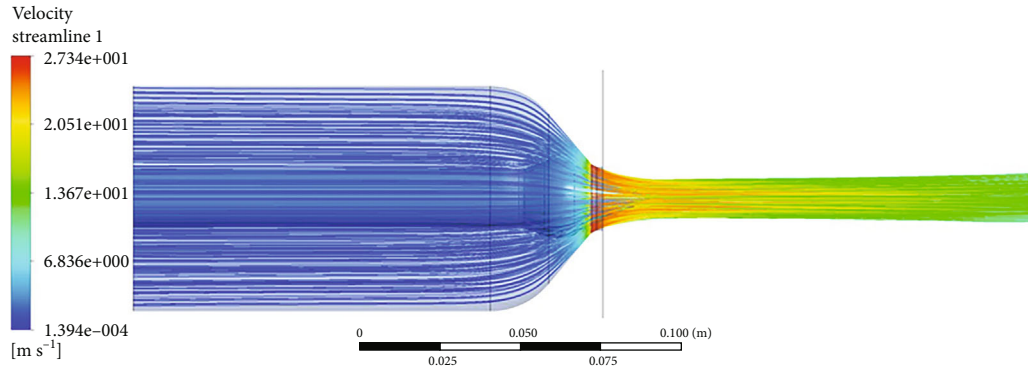

Figure 8: Flow streamline (half open nozzle).

and mesh (pre-processing), applying relevant physics to the problem at hand, and post-processing the results for valuable information. Pre-processing, i.e., the first step, involves developing a mesh of finite volumes by dividing the geometry into small volumes (Domain Discretisation) and applying the initial/boundary conditions, geometric constraints, and material properties. A 3D CAD software CATIA was used to model the surface topology better. Better modelling of surface topology eases the mesh generation process. Since the flow domain is three-dimensional and axisymmetric, a slice was modelled and used to generate the whole domain. The meshing of the flow field was done in ICEM CFD 18.2. The fine mesh was used near the walls (spear and nozzle) to capture fluid flow's viscous layer effects (boundary layer). Thus, O-grid is the efficient choice with the fine mesh on either side of the flow. Figure 7 shows the boundary condition and representative mesh for this study.

The second step discretises Navier-Stokes's equation, a second-order partial differential equation (PDE) set, which mathematically expresses the fluid flow in this study. The equations are reduced to a simple algebraic form that numerical iterations can solve for primary variables. Table 1 summarises the solver settings for steady-state flow modelling. Based on the literature, the realisable k-epsilon turbulence model is preferred. Post-processing is the final step which is analysing the solution for values of parameters of interest, assessing the validity of the primary parameters' numerical values, and examining other parameters' values.

2.2.1. Mesh Sensitivity Study. Numerical techniques are always associated with discretisation errors; hence, estimating the error related to numerical modelling is necessary. The Grid Convergence Index (GCI) method proposed by Celik et al. [28] has been used to estimate the discretisation error for the jet velocity and the erosion rate density. For h representing the grid size and subscript denoting the mesh ($h_1 < h_2 < h_3$), grid refinement factor (r) is calculated as the ratio of consecutive grid size. The following equations are used to evaluate the grid size (h), apparent order (p) of this method, extrapolated values (${\phi^{21}}_{\text{ext}}$ and ${\phi^{32}}_{\text{ext}}$), approximate relative errors (${e^{21}}_{a}$ and ${e^{32}}_{a}$), extrapolated relative errors

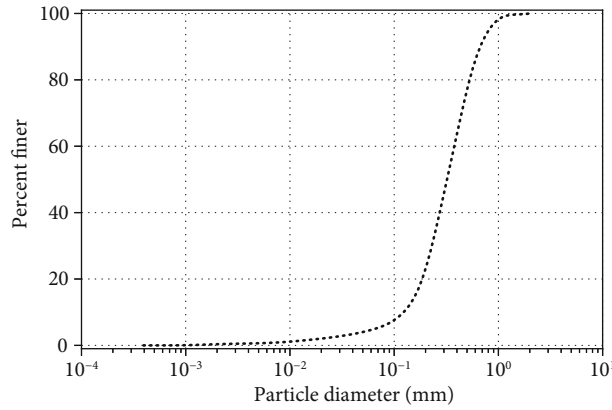

Figure 9: Particle size distribution of sand sample.

Table 3: Mineral content analysis.

Minerals		Mineral content in sand sample (%)			Average (%)	Hardness (Moh's scale)
		1	2	3		
Quartz		72	74	76	74	7
Feldspar		4	3	2	3	6
Mica		11	9	10	10	2-3
Other	A	3	5	4	4	≥5
	B	10	9	8	9	<5

Other A: tourmaline and garnet. Other B: carbonate (~5%), clay, organic matters, and a few unidentified sediments.

(${e^{21}}_{\text{ext}}$ and ${e^{32}}_{\text{ext}}$), and Grid Convergence Indices (${\text{GCI}^{21}}_{\text{fine}}$ and ${\text{GCI}^{32}}_{\text{fine}}$).

$$h = \left[\frac{1}{N}\sum_{i=1}^{N}(\Delta V_i)\right]^{1/3},$$

$$r = r_{21} = r_{32} = \frac{h_2}{h_1} = \frac{h_3}{h_2},$$

$$p = \frac{1}{\ln(r)}\left|\ln\left|\frac{\phi_3 - \phi_2}{\phi_2 - \phi_1}\right|\right|,$$

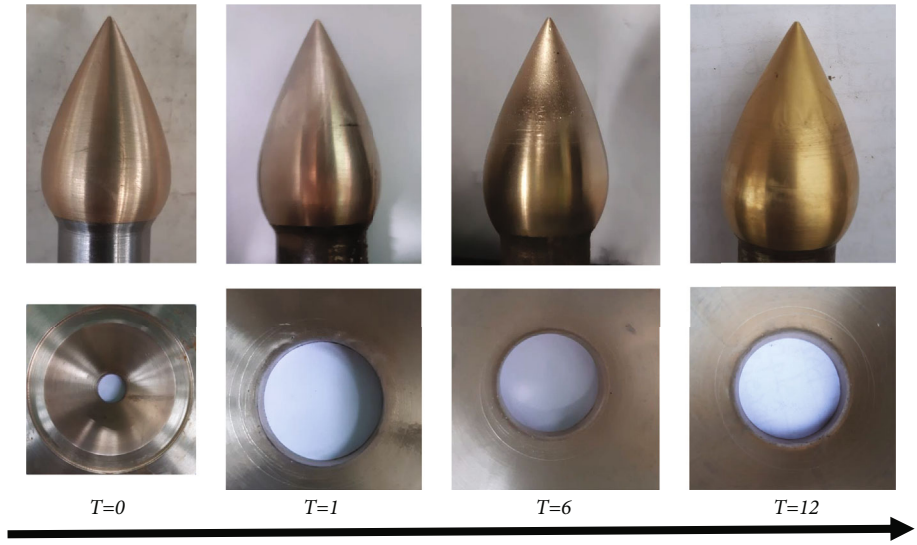

Figure 10: Needle and nozzle erosion at 50% opening at a fixed time interval (time in hrs.)

$$\phi_{\text{ext}}^{21} = \frac{r^p\phi_1 - \phi_2}{r^p - 1}; \phi_{\text{ext}}^{21} = \frac{r^p\phi_2 - \phi_3}{r^p - 1},$$

$$e_a^{21} = \left|\frac{\phi_1 - \phi_2}{\phi_1}\right|; e_a^{32} = \left|\frac{\phi_2 - \phi_3}{\phi_2}\right|,$$

$$\text{GCI}_{\text{fine}}^{21} = \frac{1.25e_a^{21}}{r^p - 1}; \text{GCI}_{\text{fine}}^{32} = \frac{1.25e_a^{32}}{r^p - 1}. \quad (1)$$

The variables selected for uncertainty analysis in the numerical calculation are the jet velocity at the region of jet-bucket interaction and the erosion rate density in the needle. Table 2 shows the discretisation error summary.

2.2.2. Flow Modelling. Figure 8 shows the streamline of flow exiting the injector obtained from the simulation. An ideal jet is supposed to have uniform velocity distribution in each cross-section with a constant jet diameter without any contraction or expansion [29]. However, experimental investigations of the jet [13, 16] reveal that the real jet deviates from this ideal form. After exiting the nozzle, the real jet first contracts and then expands. Photographic observations [13] for jet profile visualisation and Laser Doppler Anemometry (LDA) observations for understanding velocity distribution across the jet [16] are commonly employed techniques to understand the behaviour and characteristics of a real jet. Bajracharya et al. [11] have published the results of the jet contraction obtained from the numerical simulation compared with the experimental data of Staubli & Hauser [13]. Photographic observations and observations from numerical simulations are similar.

3. Results and Discussion

3.1. Sediment Sample Analysis. The quantitative (particle size distribution) analysis of the extracted sediment reveals that most of the particles (>90%) are less than 1 mm in diameter (see Figure 9). Since the sediment sample was taken at the start of the headrace tunnel, it can be inferred that these tiny particles are responsible for hydroabrasive erosion. The qualitative (mineral composition analysis) reveals the presence of quartz, feldspar, mica, tourmaline, garnet, and clay in the sediment sample (see Table 3). Among these, at 74%, quartz is the most abundant mineral. Feldspar, tourmaline, and garnet are also hard minerals with a hardness on Moh's scale equal to or greater than the hardness of turbine material which is 6 on Moh's scale [18]. The percentage of hard minerals that can erode the turbine material upon impingement is about 81%.

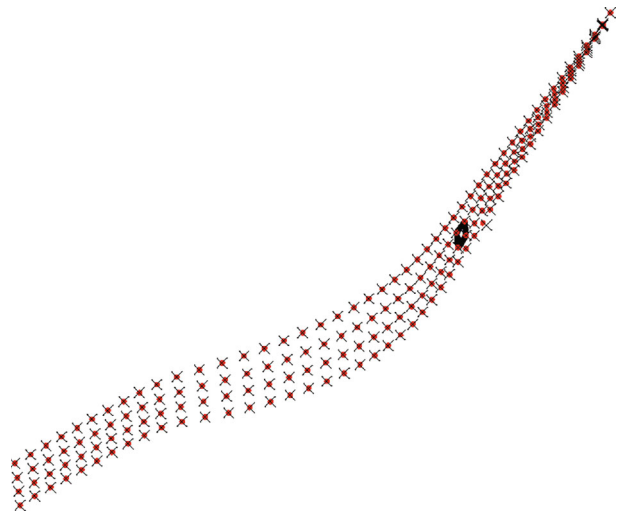

Figure 11: Needle eroded profile (red dots) and uneroded profile (black crosses).

3.2. Erosion Modelling

3.2.1. Experimental Modelling. The injector assembly was reinstalled onto the test rig after the initial measurements, and the test rig operated with a controlled feed of sediments. Images of the needle and the nozzle were taken after 1, 6,

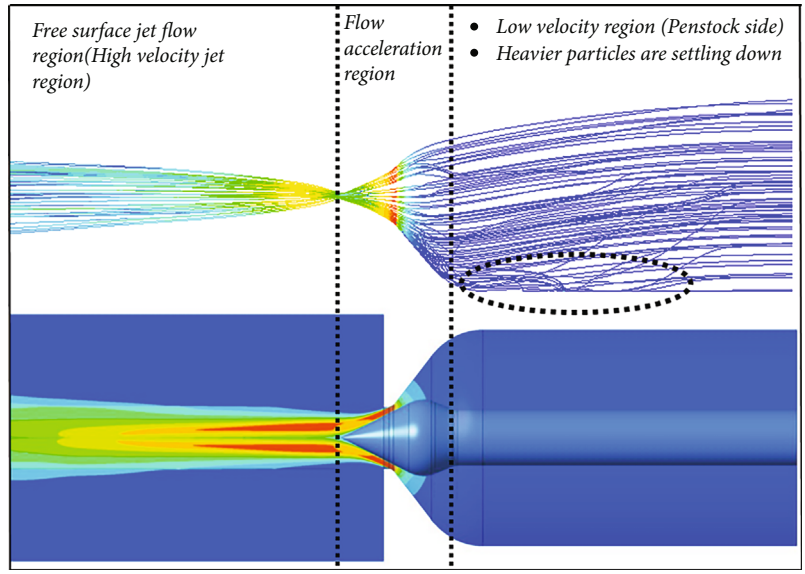

Figure 12: Sand particle tracking (50% flow rate).

Table 4: Error in the prediction of erosion rate density.

	Parameter	Value	Unit
Experimental modelling	Mass	9.77×10^{-4}	kg
	Time	21600	s
	Area	1.46×10^{-05}	m^2
	Erosion	3.09×10^{-03}	$kg/m^2.s$
Numerical modelling	Maximum erosion rate density	4.05×10^{-03}	$kg/m^2.s$
	Error	31%	

and 12 hours of operation on sand-laden water. After 12 hours of run time, the erosion was measured using the methodology described in the previous section. Images grabbed in due course of operation are summarised in Figure 10. The eroded profile of the needle was measured as illustrated in Figure 4. Figure 11 shows the comparison of initial and eroded needle profiles.

3.2.2. Numerical Modelling. Sand particles were introduced normal to the inlet surface for the case of 50% needle opening after the flow converged in ANSYS Fluent. The inlet mass flow rate of sand particles was $3.1759 * 10^{-4}$ kg/s. In total, 77,000 sand particles were tracked, among which 1,400 particles could not escape the flow domain. Visualizing the particle trajectory by particle tracking (Figure 12) reveals why those particles could not escape the flow domain. The particle tracking shows that the flow velocity is uniform upstream of the injector's convergent section, and a few particles are settling just upstream of the convergent section. The area of nozzle exit is the region of maximum particle velocity. The particle trajectory then crosses over its opposite side particle's trajectory intersecting near the nozzle tip.

3.2.3. Mass Loss Computation and Calculation. A volume region was created for the experimental calculation of the mass lost due to erosion. The black dots from Figure 11 form a volume representing the eroded needle, whereas the red dots form a volume representing the uneroded needle. The difference between these two volumes is the volume of needle material lost to erosion and thus the region of concern. The maximum erosion rate density estimated from this process is calculated and compared with CFD results in Table 4.

From the above comparison of erosion rate density, the Oka model has predicted the erosion rate density with an error of 31%.

3.2.4. Comparison of Results. Figure 13 compares the needle and the nozzle erosion from the experiment and the simulation based on the Oka model. The result shows needle tip erosion and erosion in the region between nozzle exit and needle tip. The needle seat seems to be an erosion-prone area. Similar results for the nozzle and the needle can be seen in the experimental literature [18, 20].

3.3. Effect of Injector Erosion on Jet Flow. Figure 14 shows the quantitative comparison of maximum erosion rate density in

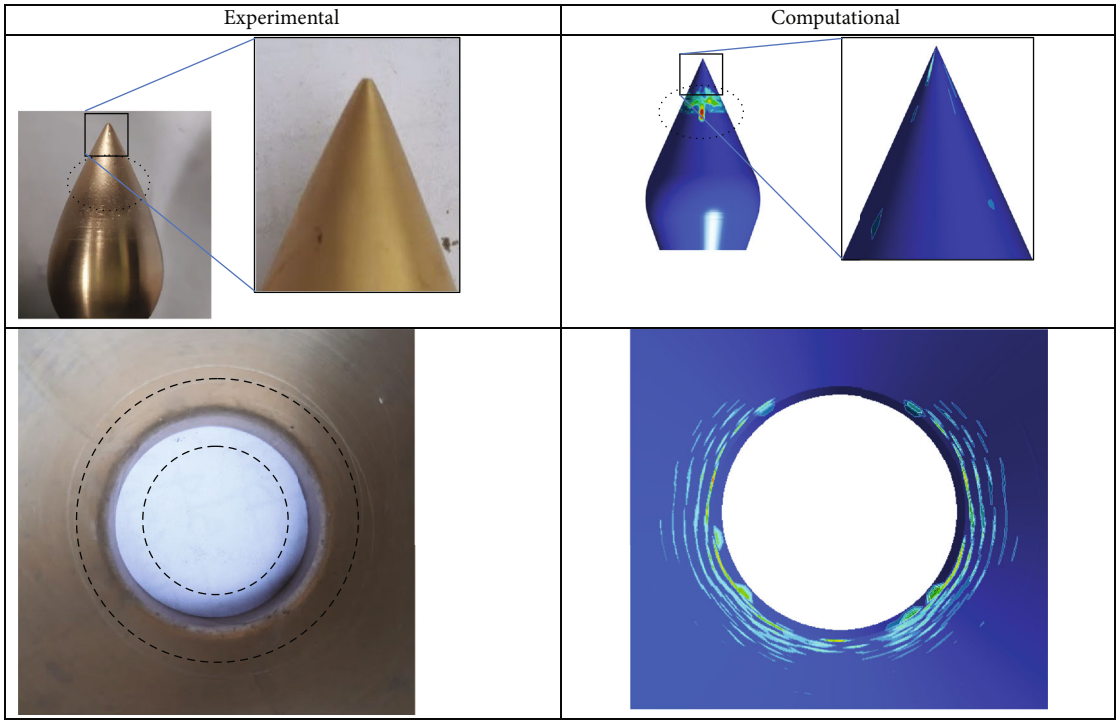

Figure 13: Comparison of needle and nozzle Erosion (after 12 hrs of operation).

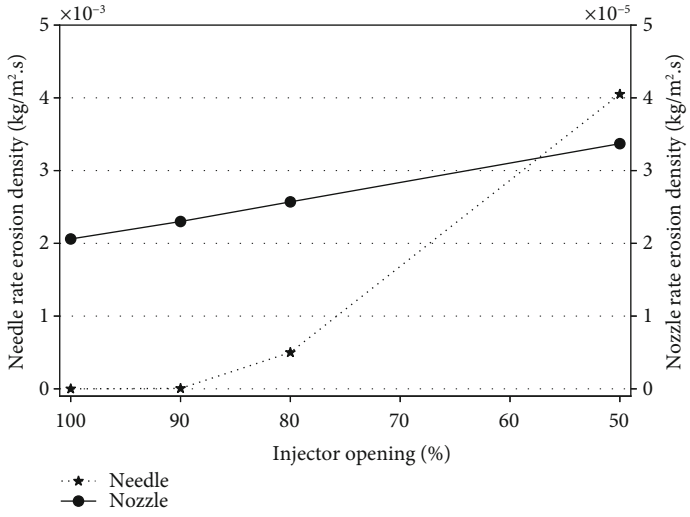

Figure 14: Erosion rate of needle and nozzle for different nozzle opening.

the needle and the nozzle for various nozzle openings, excluding tip erosion. A high rise is seen in the needle erosion rate as the nozzle closes, but there is no such sharp rise as in the case of the needle. A fully open injector shows no sign of needle erosion, whereas the erosion is severe for 50% opening. Figure 15 details the erosion of the needle and the nozzle at various injector openings. On a partially open injector, there is a danger of needle erosion. For 80% injector opening, the needle erosion initiates, whereas for 50% opening, the needle erosion is severe in the region between the needle tip and nozzle exit. Also, the nozzle erosion spreads towards the penstock pipe with a partial opening. Figure 16 shows the erosion rate density obtained from the simulations. Oka model is used for discrete phase (sand particles) modelling as discussed earlier.

3.4. Effect of Injector Erosion on Jet Flow (CFD Modelling Analysis). Wall roughness is responsible for significant losses in closed conduit flow. Erosion introduces roughness to the wall. Flow in eroded injectors was also studied from the validated CFD modelling approach. Figure 17 shows the jet velocity comparison where the jet strikes the runner bucket.

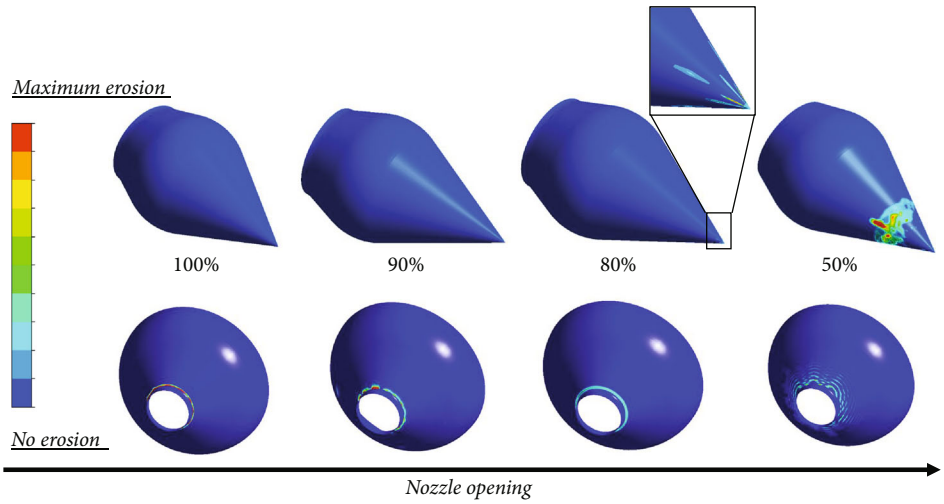

Figure 15: Needle and nozzle erosion upon various nozzle opening.

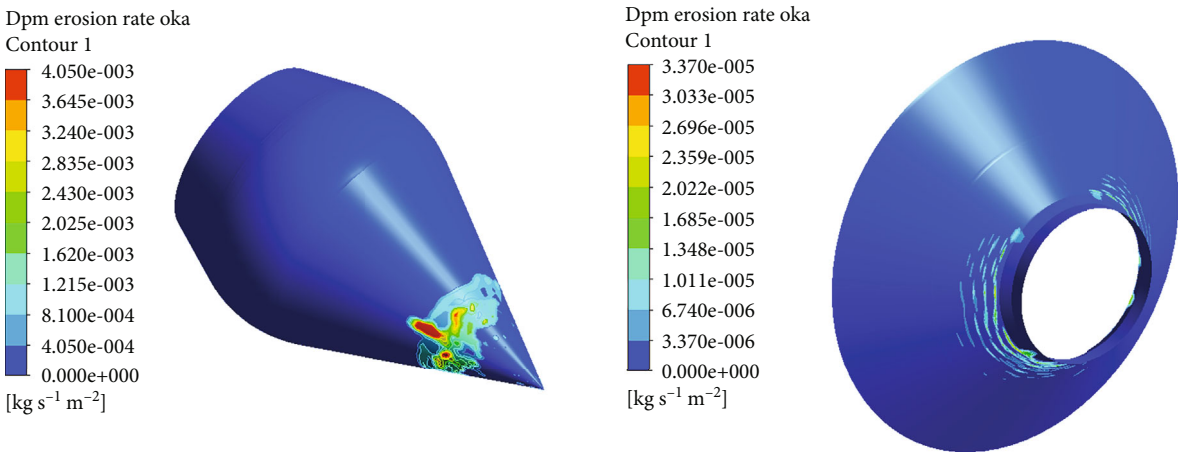

Figure 16: Erosion as predicted from CFD.

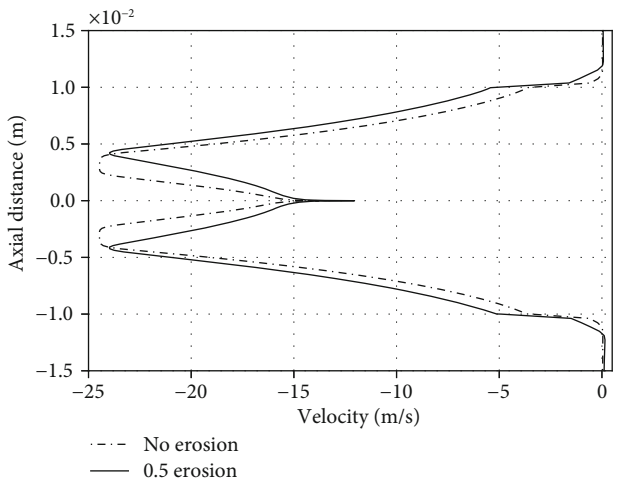

Figure 17: Jet velocity comparison for eroded and uneroded injector.

It can be seen how erosion alters the jet quality, and the shift of maximum velocity occurs. In addition, the region of maximum velocity has narrowed down, and there is a reduction in maximum jet velocity. This reduction of jet velocity affects the power production by the Pelton turbine unit. Table 5 shows the quantitative analysis of loss in jet energy due to erosion. The CFD modelling reveals that uniform erosion of 0.5 mm on the erosion-prone area results in a 5.63% loss in jet energy.

Hydromechanical components' erosion is associated with energy loss due to leakages, secondary flow, or an increase in head loss due to rough surfaces. As a result of erosion, the turbine's water consumption rate at a particular load (power produced) increases more than the rated flow for that particular load. This phenomenon causes reduced average load (MW) of run-of-the-river (ROR) plants and an increased rate of reservoir water level depletion in storage and peaking run-of-the-river (PROR) plants. In addition, an increase in head loss due to the rough surface causes reduced efficiency of the generating units. Both of the cases are associated with decreased revenue for the plant. Thus, it is always desired that hydropower plants operate in the economic zone concerning operating conditions of generating units, erosion potential of the water, and energy losses in the machine due to erosion.

Numerical analysis of different types of spear-nozzle arrangements is possible with the method presented in this study. This type of study can be done to predict erosion-prone areas, erosion rate density (kg/m^2/s), mass lost (kg) at different operating hours, and relative energy losses (%) with different erosion rates (mm). It can be possible to operate the Pelton turbine injector in its economical operating zone by properly establishing operating rules and computing the above parameters. Development of the proposed method is possible by adding a field setting research to the numerical and experimental modelling. The proposed method can be further developed by investigating actual erosion and flow behaviour in a Pelton turbine plant.

In addition, injector erosion causes alteration of the specially shaped needle-nozzle profile, causing leakage of a significant volume of water even though the control servomotor fully closes the injector. This leakage makes the pressure balance on both sides of the Main Inlet Valve (MIV) unachievable. Due to this pressure imbalance, operators experience difficulties in opening the MIV. Also, the rotating components in the Pelton turbine come into motion even at 0% injector opening, which disturbs the operating sequence of the generating units. Both the cases are undesired for the safe operation of a Pelton turbine unit. As safety is a significant concern, tracking water leakage with changing shape morphology of spear-nozzle arrangement is paramount. Different types of needle valves (comprising of needle-nozzle arrangement) are used in the hydropower industry for flow control. One such application area is a bypass valve for filling the distributor and balancing pressure on the other side of the MIV before its opening. Water leakage from a bypass valve with a leaking distributor is a loss of water hence the plant revenue. Thus, the method proposed can also be employed to establish an operating rule for the bypass valves, allocating optimal time to overhaul or replace the valve, ensuring minimal or zero water leakage.

Table 5: Alteration of jet velocity and loss of energy.

Item	Value	Units
Before erosion (blue line)	24.5	m/s
After erosion (red line)	23.8	m/s
Energy of jet	$E = \frac{1}{2}Qv^2$	J
Loss in energy	5.63%	

It is now possible to track the changing shape morphology of spear-nozzle arrangement with different operating hours by developing similitude models and employing the methods discussed in this article. Deploying such tracking methods allows us to realise any shape change in spear-nozzle arrangement and potential leakages into the turbine runner unit leading to safety hazards. This knowledge can then be used to establish an operating rule for the generating units for allocating time to overhaul the injector, ensuring safe operation.

4. Conclusion and Recommendations

It is understood that erosion of turbine parts causes various undesired effects. A few significant effects are listed below:

(i) Due to mass imbalance, mechanical vibration in rotating parts (especially turbine runner/s) is introduced

(ii) Due to force imbalance, mechanical vibration in stationary parts (especially distributor part/s) is introduced

(iii) Due to the change in surface roughness, the smooth surface turns into a rough surface, causing more head loss

(iv) Due to the surface morphology change, leakage and secondary flows are introduced in the flow conduits, causing unwanted vortices. These vortices cause energy losses and mechanical vibrations and enhance erosion

(v) The erosion of distributor parts (guide vane or injector) causes alteration of the specially shaped guide vane profile and needle-nozzle profile, causing water leakage even though the governor fully closes the distributor. Because of this leakage, pressure equilibrium on both sides of the Main Inlet Valve (MIV) may not be achieved, and turbine operators experience difficulty opening the MIV. In addition, after opening the MIV, the leakage causes turbine parts to rotate without opening the distributor

(vi) In the case of the Francis turbine, erosion of parts like the head cover and bottom ring causes leakage from the machine to the powerhouse floor, causing a dramatic increase in the drainage pit filling rate.

This process causes sediment filling in the pit, overloading, and frequent breakdown of the emptying pumps

Understanding the nature and effect of sand particle-led erosion of Pelton turbine injectors is vital for preventing vibrations and energy losses. Identifying leakage areas for the safe operation of the hydropower plant is an equally important reason to study and predict erosion. In this study, the erosion in the Pelton turbine injector was experimentally analysed using a dry sand test rig and numerically using a commercial CFD code with the Oka model. Sand samples collected from the outlet of the desanding basin (entrance of head race tunnel) of a hydropower plant operating in the Chilime River, Nepal, were collected for this study. The analysed sand sample revealed the maximum size of the sand particle to be 2 mm, with the presence of 81% hard minerals (hardness more than 5 on Moh's scale). The particle size distribution obtained from lab tests is adopted for numerical simulation replicating the environment similar to the experiments.

Similarly, three different controlled sand flow rate (74%, 3%, and 5%) is maintained in the test rig to replicate different concentration of the hard minerals (quartz, feldspar, tourmaline, and garnet) in the hydropower. It is assumed that softer particles do not cause erosion. Numerical modelling of the sand particle-led erosion in the injector was done, considering the injector as a flow control device with the Oka erosion model. The key findings of this research work are as follows:

(i) The erosion-prone area was simultaneously identified as the needle surface between the tip and nozzle exit from experimental, numerical, and field studies. More specifically, from visual observation of the brass injector after 6 hours of operation (experimental), it was revealed that

  (i) The needle erosion was maximum between the needle tip and nozzle exit

  (ii) The nozzle erosion was maximum in the needle seat

  (iii) The needle tip blunted

(ii) Experimental computation of the needle erosion rate density (mass lost per unit area per unit time) was done by shape mapping and Boolean subtraction of eroded and noneroded needle shapes after 6 hours. With a comparison of erosion patterns between experiments and computations, an error of 31% was seen from the quantitative comparison of erosion rate density. This error is accounted to different factors

  (i) The occurrence of cavitation is not considered in numerical modelling

  (ii) Different shapes of minerals like quartz, feldspar, and hard minerals (tourmaline and garnet) are assumed to be round in numerical modelling without accounting for sphericity

  (iii) Experimental measurement errors

(iii) The severity of erosion increases with a partially opened injector. There is an increase in the erosion rate density of the needle, and the erosion in the needle seat (or nozzle) spreads throughout the whole nozzle body. It is thus recommended to operate the Pelton turbine unit at fully open conditions as far as applicable to minimize erosion

(iv) Numerical modelling shows that with the imposition of the injector's flow accelerating area (also the erosion-prone area), a comparison of jet energy shows a loss of 5.63%. The erosion of 0.5 mm is evenly spread

The authors of this article are now interested and recommend the following for further studies in flow and erosion modelling in Pelton turbine injector:

(i) The injector converts the potential energy of water to kinetic energy in the form of a high-speed jet. During this conversion process, a flow acceleration region is formed in the injector (see Figure 12). During this acceleration, there are chances of flow separations in the region which only exacerbates after the erosion inception on the spear-nozzle surface. This flow separation invites cavitation in the Pelton turbine injector. The water bubbles move with the high-speed jet and collapse on the bucket surface, causing pitting. To fully understand the phenomenon, its effect, and combating technique, the occurrence of cavitation in the Pelton turbine injector must be predicted

(ii) It is well known that crystal shapes of different minerals like quartz, feldspar, and hard minerals (tourmaline and garnet) constituting the sediment carried by rivers originating from the Himalayas region are different. There is a difference in crystalline shape, density, and hardness, so they have different erosion potential. Further development in the numerical modelling techniques of sand particle flow is critical. One such approach can be dividing the sand particle flow per the sand mineralogical composition with different shape factors by introducing shape factors in numerical models to minimize the error

(iii) A computer-based three-dimensional scanning technique can minimise error in experimental modelling and tracking shape morphology changes of turbine parts with operating hours

Data Availability

The data used to support the findings of this study are included in the article.

Conflicts of Interest

The authors declare that there are no conflicts of interest regarding the publication of this paper.

Acknowledgments

The authors would like to acknowledge University Grants Commission, Sanothimi, Bhaktapur, for funding this research under Faculty Research Grant (Grant No.: FRG-74/75-Engg-04). Technical support from Centre for Energy Studies (Institute of Engineering), Chilime Hydropower Plant, and Robotics Club (Pulchowk Campus) are highly acknowledged.

References

[1] H. P. Pandit, "Sediment handling at run-of-river projects in Himalayan rivers using sediment rating curves," *Nepalese Journal of Engineering*, vol. 1, no. 1, pp. 39–45, 2005.

[2] L. Poudel, B. Thapa, B. P. Shrestha, B. S. Thapa, K. P. Shrestha, and N. K. Shrestha, *Computational and experimental study of effects of sediment shape on erosion of hydraulic turbines. IOP Conference Series: Earth and Environmental Science*, 26th IAHR Symposium on Hydraulic Machinery and Systems (Vol. 15), 2012.

[3] T. R. Bajracharya, B. Acharya, C. B. Joshi, R. P. Saini, and O. G. Dahlhaug, "Sand erosion of Pelton turbine nozzles and buckets: a case study of Chilime Hydropower Plant," *Wear*, vol. 264, no. 3-4, pp. 177–184, 2008.

[4] B. Thapa, *Sand Erosion in Hydraulic Machinery*, Norwegian University of Science and Technology, 2004.

[5] A. Chhetri, R. B. Kayastha, and A. Shrestha, "Assessment of sediment load of Langtang River in Rasuwa District, Nepal," *Journal of Water Resource and Protection*, vol. 8, no. 1, pp. 84–92, 2016.

[6] B. Chhetry and K. Rana, "Effect of sand erosion on turbine components: a case study of Kali Gandaki "A" hydroelectric project (144 MW), Nepal," *Hydro Nepal: Journal of Water, Energy and Environment*, vol. 17, pp. 24–33, 2015.

[7] H. P. Neopane and S. Sujakhu, "Particle size distribution and mineral analysis of sediments in Nepalese hydropower plant: a case study of Jhimruk hydropower plant," *Kathmandu University Journal of Science, Engineering and Technology*, vol. 9, no. 1, pp. 29–36, 2013.

[8] M. K. Padhy and R. Saini, "Effect of size and concentration of silt particles on erosion of Pelton turbine buckets," *Energy*, vol. 34, no. 10, pp. 1477–1483, 2009.

[9] D. Felix, I. Albayrak, A. Abgottspon, and R. M. Boes, "Hydro-abrasive erosion of hydraulic turbines caused by sediment - a century of research and development," *IOP Conference Series: Earth and Environmental Science*, vol. 49, article 122001, 2016.

[10] H. Brekke, Y. Wu, and B. Cai, "Design of hydraulic machinery working in sand laden water," in *Abrasive Erosion and Corrosion of Hydraulic Machinery*, C. G. Duan and V. Y. Karelin, Eds., vol. 2, pp. 155–181, Imperial College Press, London, 2002.

[11] T. R. Bajracharya, R. Shrestha, and A. B. Timilsina, "A methodology for modelling of steady state flow in Pelton turbine injectors," *Journal of the Institute of Engineering*, vol. 15, no. 2, pp. 246–255, 2020.

[12] T. Nonoshita, Y. Matsumoto, T. Kubota, and H. Ohashi, "Numerical simulation of jet in a Pelton turbine," *Hydraulic Machinery and Cavitation*, vol. 352–360, 1996.

[13] T. Staubli and H. P. Hauser, "Flow visualization - a diagnosis tool for pelton turbines," *IGHEM2004, Lucerne, Switzerland*, vol. 1, pp. 1–9, 2004.

[14] M. Peron, E. Parkinson, L. Geppert, and T. Staubli, "Importance of jet quality on Pelton efficincy and cavitation," *IGHEM 2008 – MILANO 3rd-6th September International Conference on Hydraulic Efficiency Measurements*, pp. 1–9, 2008.

[15] V. Gupta and V. Prasad, "Performance analysis of nozzles used in impulse hydraulic turbines using CFD," *Proceeding of National Conference on Fluid Mechanics and Fluid Power, College of Engineering, Pune*, pp. 1–8, 2009.

[16] Z. Zhang and M. Casey, "Experimental studies of the jet of a Pelton turbine," *Proceedings of the Institution of Mechanical Engineers, Part A: Journal of Power and Energy*, vol. 221, no. 8, pp. 1181–1192, 2007.

[17] T. R. Bajracharya, *Efficiency Deterioration in Pelton Turbines Due to Sand-Particle-Led Bucket Erosion*, Tribhuvan University, 2007.

[18] H. P. Neopane, O. G. Dahlhaug, and M. Cervantes, "Sediment erosion in hydraulic turbines," *Global Journal of Research Engineering*, vol. 11, no. 6, 2011.

[19] D. Karandikar, *HVOF coatings to combat hydro abrasive erosion*, International Conference On Hydropower Sustainable Development, Dehradun, 2015.

[20] B. A. M. Morales, I. F. Pachón, U. J. Loboguerrero, J. A. Medina, and G. J. A. Escobar, "Development of a test rig to evaluate abrasive wear on Pelton turbine nozzles. A case study of Chivor hydropower," *Wear*, vol. 372-373, pp. 208–215, 2017.

[21] C. Zeng, Y. Xiao, J. Zhang, S. H. Ahn, and Z. Wang, "Numerical analysis of pelton turbine needle erosion characteristics," *Journal of Drainage and Irrigation Machinery Engineering*, vol. 33, pp. 407–411, 2015.

[22] Z. Chongji, X. Yexiang, Z. Wei, Y. Yangyang, C. Lei, and W. Zhengwei, "Pelton turbine needle erosion prediction based on 3D three- phase flow simulation," *IOP Conference Series: Earth and Environmental Science*, vol. 22, no. 5, article 052019, 2014.

[23] G. V. Messa, S. Mandelli, and S. Malavasi, "Hydro-abrasive erosion in Pelton turbine injectors: a numerical study," *Renewable Energy*, vol. 130, pp. 474–488, 2019.

[24] I. H. Jung, Y. S. Kim, D. H. Shin, J. T. Chung, and Y. Shin, "Influence of spear needle eccentricity on jet quality in micro Pelton turbine for power generation," *Energy*, vol. 175, pp. 58–65, 2019.

[25] T. R. Bajracharya, R. Shrestha, and A. B. Timilsina, "Solid particle erosion models and their application to predict wear in Pelton turbine injector," *Journal of the Institute of Engineering*, vol. 15, no. 3, pp. 349–359, 2020.

[26] A. Židonis and G. A. Aggidis, "State of the art in numerical modelling of Pelton turbines," *Renewable and Sustainable Energy Reviews*, vol. 45, pp. 135–144, 2015.

[27] D. E. Papantonis, J. S. Anagnostopoulos, and P. K. Koukouvinis, *Flow modelling in the injector of a Pelton turbine*, 4th international SPHERIC workshop, (May 2009), 2009.

[28] I. B. Celik, U. Ghia, P. J. Roache, C. J. Freitas, H. Coleman, and P. E. Raad, "Procedure for estimation and reporting of uncertainty due to discretization in CFD applications," *Journal of Fluids Engineering, Transactions of the ASME*, vol. 130, no. 7, pp. 078001–780014, 2008.

[29] Z. Zhang, *Pelton turbines*, Springer, 2016.